A Novel Integral Image Recognition Method and System with Verification Measurement by Sensors for Hot Steel-bar Stack Accident Detection

Wen Ren,[1] Kun-Chieh Wang,[1*] Long Wu,[1] Jian-Zhou Pan,[2] Hao Gao,[1] and Yao Li[1]

[1]School of Mechanical and Electric Engineering, Sanming University, Sanming, Fujian 365004, China
[2]Fujian Provincial Sansteel (Group) Co., Ltd., Sanming, Fujian 365000, China

Bar-type steel is commonly used in engineering facilities, which is made from the raw material of steel wire with high-speed rolling. A hot steel-bar stack (HSBS) accident is a serious accident wherein a hot steel bar flies out from a bar stack fixed on a trolley during manufacturing. If not prevented on time, it can damage production equipment and cause fire and personal injury. At present, the monitoring and identification of HSBS accidents during the rolling manufacturing process are still limited to manual observation. We lack advanced monitoring and identification methods. Finding an effective, accurate, and rapid identification method as well as a treatment method for detecting an HSBS accident in the rolling manufacturing process is an urgent issue. To solve this problem, we propose a novel three-in-one image recognition (TIOIR) method based on the bagging and boosting ensemble learning schemes. The TIOIR method integrates the maximum distance positioning, corner detection positioning, and ablation methods to better identify different features of HSBS images. Furthermore, we designed and built a fault diagnosis system of HSBS accident detection, which includes temperature and visual sensors, visual detection devices, and a remote control and computing unit embedded with our proposed TIOIR scheme. Through the operation of the fault diagnosis system, we carried out an actual identification experiment of HSBS accident detection in the rolling field, and the obtained real-time recognition rate was as high as 97%.

1. Introduction

1.1 Hot steel-bar stack accidents

Bar-type steel is the most common profile of steel, which is usually produced by single-line high-speed rolling, as shown in Fig. 1. Hot steel-bar stack (HSBS) accidents are the most common and serious accidents in the steel rolling process, and their frequency accounts for more than half of all steel rolling accidents, as shown in Fig. 2. When an HSBS incident occurred, hot, soft steel bar flew out of a pile of steel bar secured to a cart during the production process. If this

Fig. 1.   (Color online) Steel-bar rolling site.   Fig. 2.   (Color online) HSBS accident.

type of accident cannot be prevented on time, the production equipment will be severely damaged and the production will be halted, and even personal injury will occur.[1–5]

Thus far, many studies have put forward a series of solutions to the common problem of HSBS accidents.[6–10] Rusnák *et al.*[6] proposed the method of increasing the final thickness of rolled steel to eliminate surface defects as much as possible. Dominik *et al.*[7] proposed a system that can be applied to reduce the occurrence of stacking steel accidents. By numerical simulation, Pater *et al.*[8] found that the criterion based on structural stress is more suitable for predicting the fracture of rolled steel. Bouguettaya *et al.*[9] proposed a novel approach that uses an ensemble of two pretrained state-of-the-art convolutional neural networks (CNNs) to deal with the identification problem for rolled steel. Qian *et al.*[10] established a new differential eddy-current method for classifying the raw materials of steel bars.

How to effectively detect HSBS accidents and take appropriate measures have become urgent problems that need to be solved. At present, machine vision methods based on various advanced and accurate recognition schemes such as the recurrent neural network, deep neural network, and CNN can effectively and accurately monitor harsh working environments and are suitable for this study.[11–15]

1.2   Machine vision technology for detecting HSBS accidents

For HSBS accident detection, the human vision inspection method was commonly used. However, this method has extremely low efficiency and lacks reliability. Instead, currently, the machine vision method with advanced recognition schemes is widely used for inspection works. However, how to use machine vision methods to improve the accuracy and efficiency of image recognition is still challenging, especially with little research on HSBS accident detection.[16–18] Abhishek and Jegadeeshwaran[19] invented a new machine learning method to investigate the problems of classifying and predicting tool states. Yanzhou *et al.*[20] summarized the machine learning algorithms for detection in the process of metal laser-based additive manufacturing. In their study, the machine learning scheme, defect type, data type, material type, and calculation accuracy used in the laser-based additive manufacturing process were discussed.[20] Khan *et al.*[21] developed a learning model based on the CNN scheme to detect real-time malicious

defects to reduce human involvement for checking product quality in manufacturing. This approach adopted the concepts of image classification and computer vision via machine learning, which is a popular technology for detecting the causal relationships of defects. Goyal *et al.*[22] used the support vector machine and artificial neural network schemes to identify and classify bearing defects. Benbarrad *et al.*[23] proposed a model containing various integrated machine learning schemes in the production chain to identify the data pattern and suggested corrective actions to ensure product quality during manufacturing.

On the basis of the vast merits of using machine learning schemes in the defect detection and classification of engineering products, we propose a three-in-one image recognition (TIOIR) method based on a machine learning scheme to solve the problem encountered in HSBS accident detection.

2. HSBS Accident Identification Methodology and System

2.1 Identification methodology

To better identify and further prevent HSBS accidents in a steel-making plant, we propose a methodology including four manipulation procedures for the image recognition of HSBS accidents. First, on the basis of the practical industrial network architecture of a steel-rolling manufacturing site, we designed an image detection and identification system for HSBS accidents. Second, we used the maximum gray-scale and median-filter methods to catch the red and hot steel bar features of collected images and reduce overall data noises. Third, for feature recognition and classification, we studied and compared three advanced methods, namely, the maximum-distance positioning method based on the Hough transform (MDPHT),[24] the positioning method based on the Harris corner detection (PHCD),[25] and the curvature-recognition algorithm based on the ablation scheme (CRA).[26] Fourth, we combined the merits of the previous three methods and proposed a novel TIOIR method on the basis of the bagging and boosting ensemble learning scheme[27] to improve the final identification accuracy of HSBS accidents.

2.2 Identification system

To effectively detect the HSBS accidents in the rolling manufacturing process, we built an identification system, as shown in Fig. 3, which includes the following six parts: the detecting unit (visual and infrared thermal image sensors), the data processing unit, the data transmitting unit (Ethernet and data exchanger), the data manipulation unit (cloud servers and cloud computers), an alarm unit, and a remote central control unit. The former three units constitute a detection subsystem, and we have four subsystems in total to obtain the images of various HSBS accidents in real time, which are set at the sites of rough rolling, middle rolling, pre-fine rolling, and fine rolling.
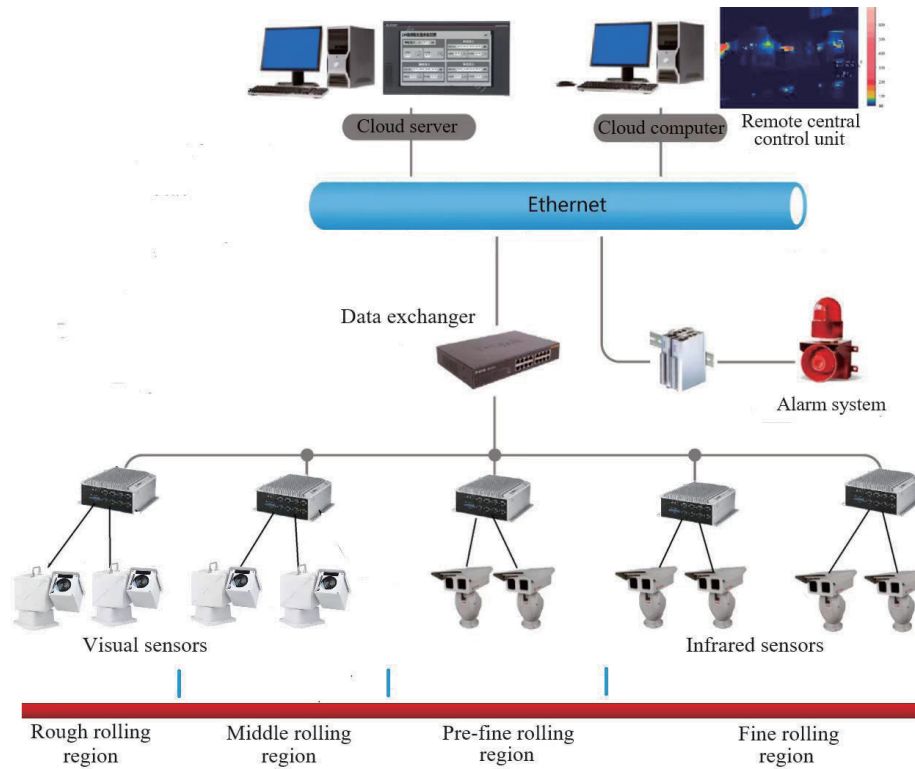
Fig. 3. (Color online) Detection and identification system for detecting HSBS accidents in rolling manufacturing process.

3. Image Detection and Preprocessing

3.1 Image detection and temperature sensing

We adopted the detection and identification system established above. We used an infrared thermal image sensor and a vision sensor [Fig. 4(a)] to detect and capture physical images and the temperature distributions of HSBS accidents, respectively. The obtained typical results are respectively shown in Figs. 4(b) and 4(c).

3.2 Image preprocessing

The steel rolling environment is full of clutter items, such as crud, dust, and pollutants. This type of highly dirty and harsh environment causes the images of HSBS accidents taken by visual sensors to become vague and noisy, which are difficult to distinguish. The interference factors include various surrounding lights, scattered lights reflected by water stain, discrete hot spots caused by the high-temperature environment, and noise disturbances caused by machine vibration. To improve the accuracy of extracting crucial features from the images of HSBS accidents, it is necessary to develop appropriate preprocessing and feature extraction schemes.
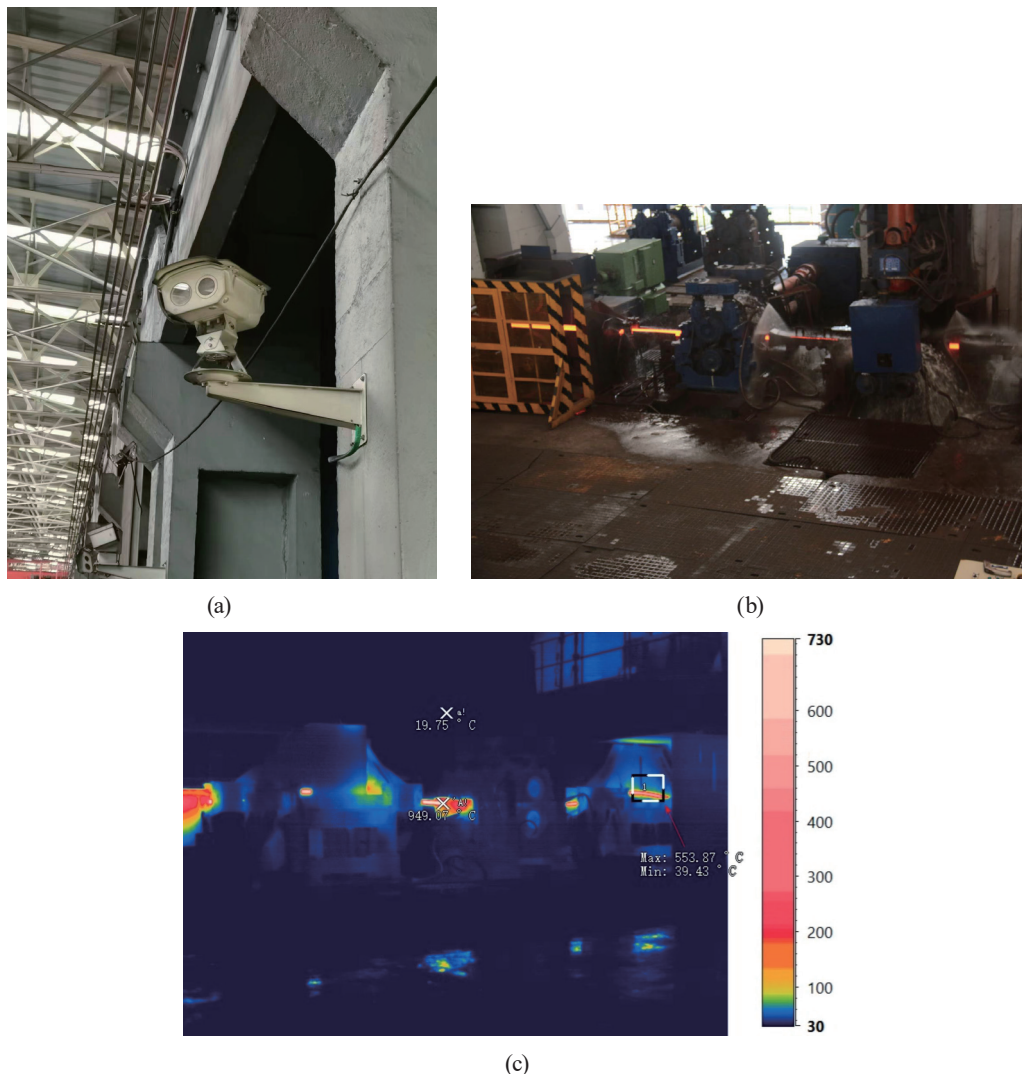
Fig. 4.   (Color online) Image detection and temperature sensing: (a) infrared thermal image sensor, (b) image of HSBS accidents obtained by a visual sensor, and (c) temperature distributions of HSBS accidents obtained using an infrared thermal image sensor.

The obtained typical image of HSBS accidents with interference by clutter items is shown in Fig. 5(a) and that with interference by noisy lights is shown in Fig. 5(b). Focusing on these two typical images of HSBS accidents, we next performed the image data preprocessing, which is divided into the image gray-scaling and the image filtering.

3.2.1   Image extraction

To find a proper way of better extracting the images of HSBS accidents, we analyzed three commonly used methods: the maximum gray-scale method, the mean gray-scale method, and the component method.[28] These methods are capable of eliminating the image ambiguity caused by similar backgrounds. We applied these methods to analyze the image shown in Fig. 5(a) and the obtained results are shown in Fig. 6(a) (extracted by the maximum gray-scale

(a)   (b)

Fig. 5. (Color online) Images of HSBS accidents: (a) interference by cluster items and (b) interference by noisy lights.

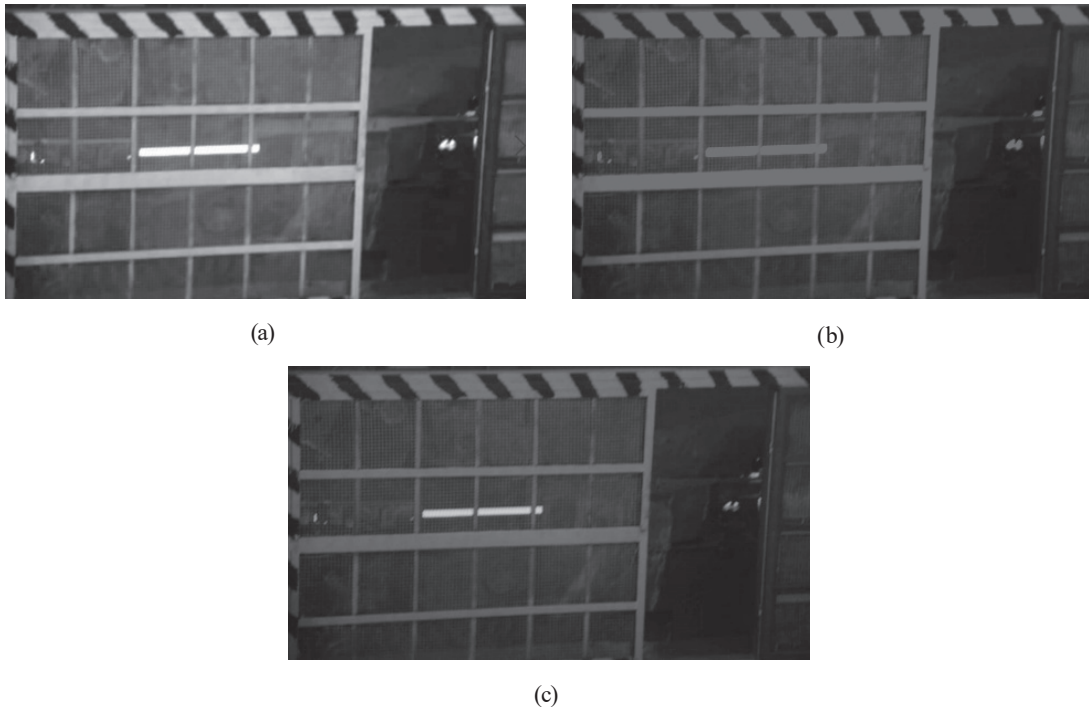(a)   (b)

(c)

Fig. 6. Images obtained by different extraction methods for the picture shown in Fig. 5(a): (a) maximum gray-scale method, (b) mean gray-scale method, and (c) component method.

method), Fig. 6(b) (extracted by the mean gray-scale method), and Fig. 6(c) (extracted by the component method). Comparing these three images with the original image, we found that the maximum gray-scale method has the best identification effect among all the methods.

Furthermore, we used these three methods to analyze the image shown in Fig. 5(b) and the obtained results are shown in Fig. 7(a) (extracted by the maximum gray-scale method), Fig. 7(b) (extracted by the mean gray-scale method), and Fig. 7(c) (extracted by the component method). We found from Fig. 7 that the maximum gray-scale method still has the best identification effect among all the methods, even though there exists much interference from scattering lights and
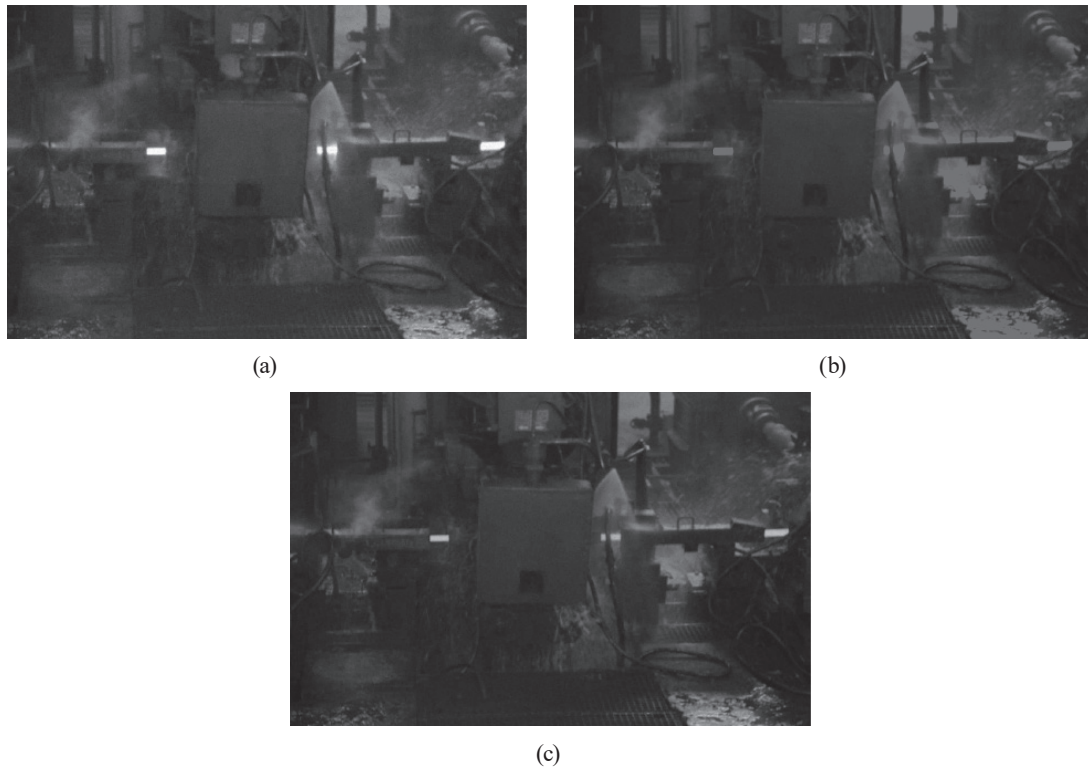
(a)   (b)

(c)

Fig. 7.   Images obtained by different extraction methods for the picture shown in Fig. 5(b): (a) maximum gray-scale method, (b) mean gray-scale method, and (c) component method.

clutter noises. Hence, we concluded that the maximum gray-scale method is excellent in data preprocessing for the identification of HSBS accidents and we adopted this method throughout this study.

3.2.2 Image filtering

The image filtering scheme is often used for the image noise reduction to obtain relatively clear images. Thus far, the most commonly used filtering schemes are mean filtering, Gaussian filtering, and median filtering.[29] The light-noise interfered image shown in Fig. 5(b) was selected as the target picture. After the extraction processing by the maximum gray-scale method, we applied the above three schemes to filter the target picture. The obtained results are shown in Fig. 8. We found that, in an overall comparative sense, the median filtering scheme has the best denoising effect among all the methods because of higher articulation.

3.3 Image feature extraction

3.3.1 Image binarization processing

To solve the problem of image confusion between the features of the red and hot rolling steel bars and their background, we further needed to introduce the image binarization (IB) scheme.

(a)   (b)
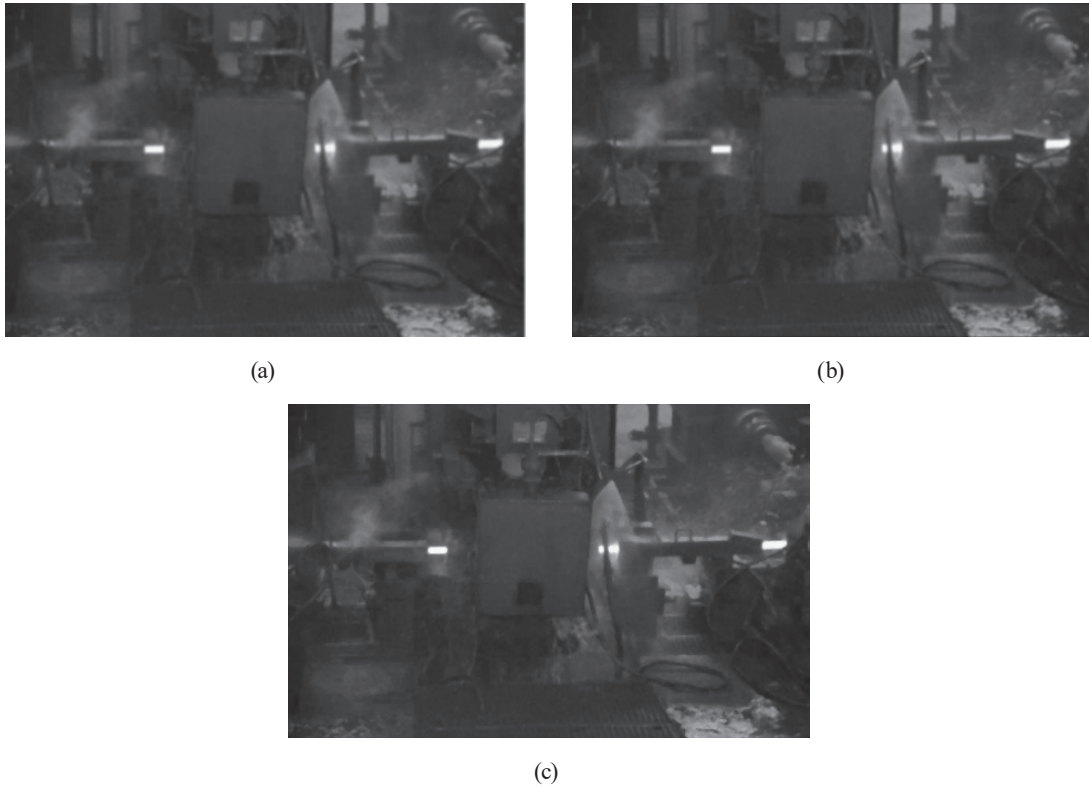
(c)

Fig. 8.   Image filtering by different schemes: (a) mean filtering, (b) Gaussian filtering, and (c) median filtering.

The IB scheme involves the data normalization and threshold segmentation.[30] The appropriate threshold in the IB scheme is closely related to the integrity of image feature extraction, which ultimately affects the classification effect. We found that a setting of the threshold as the maximum gray-scale value or within the range of 35–45 can completely separate the confusion noise from the original image. The thus-obtained HSBS images shown in Figs. 5(a) and 5(b) via the IB scheme are respectively shown in Figs. 9(a) and 9(b).

3.3.2 Image marginalization processing

We encountered two problems in the execution of the IB scheme: long calculation time and misleading information. To solve these two problems, we introduced the image marginalization (IM) scheme that mainly includes two operators: Sobel and Canny.[31] Through calculations by the IM scheme with these two operators, we obtained two edge images of Fig. 5(a), as shown in Figs. 10(a) and 10(b). We comparatively found that both operators yield clear images of the edges of the hot steel bars. Therefore, in the following case study, the IM scheme together with these two operators was adopted.
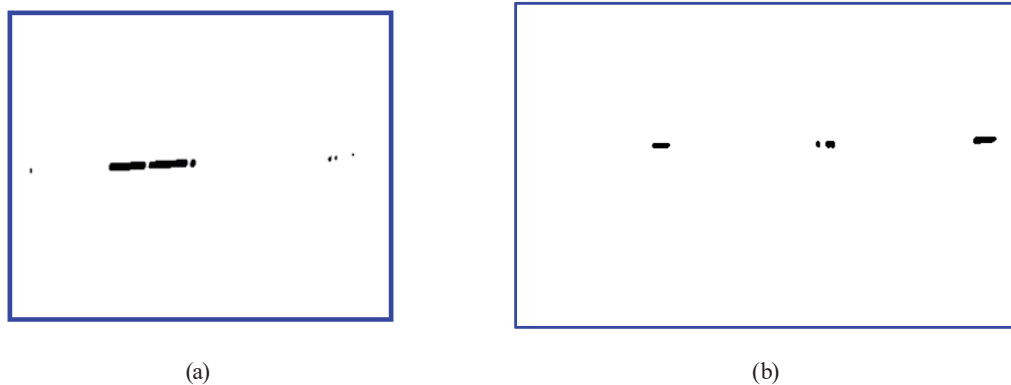
(a)   (b)

Fig. 9.   (Color online) Images after processing by IB scheme: (a) processed image of Fig. 5(a) and (b) processed image of Fig. 5(b).

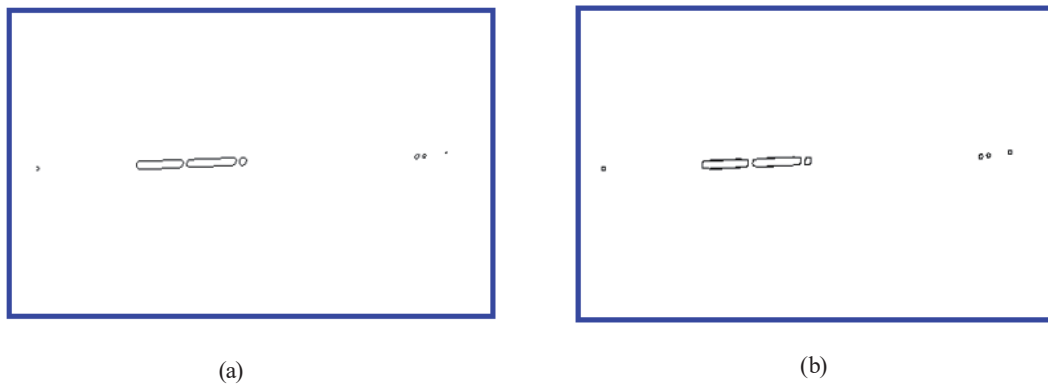(a)   (b)

Fig. 10.   (Color online) Processed edge images of Fig. 5(a): (a) image by Sobel operator scheme and (b) image by Canny operator scheme.

4.   Image Feature Recognition and Classification

To overcome the recognition difficulties caused by interference such as lens vibration, lens offset, and spark during the image acquisition via the visual sensor system at the rolling site, we introduced three advanced regional boundary-crossing (ARBC) methods to deal with the obtained images, namely, MDPHT, PHCD, and CRA.[32] In the following, the comparative analyses of these three methods were carried out and a more comprehensive identification method was developed on the basis of their combination.

4.1   MDPHT

To solve the problem that the picture taken by vision sensors usually has too many image pixels, which leads to a long calculation time, we adopted MDPHT to eliminate unnecessary image pixels. First, considering two different pictures of HSBS accidents as shown in Figs. 11(a) and 12(a), we set the point ratio (PR), which is the ratio of the point number inside the boundary to the point number at the boundary, as 0.146 and 0.107, respectively, in MDPHT calculations.
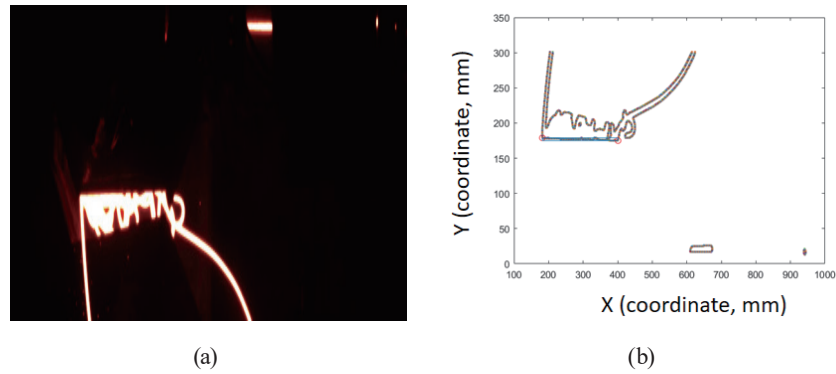
Fig. 11.   (Color online) Pictures of rolled-type HSBS accident: (a) picture taken by vision sensors and (b) picture processed by MDPHT.
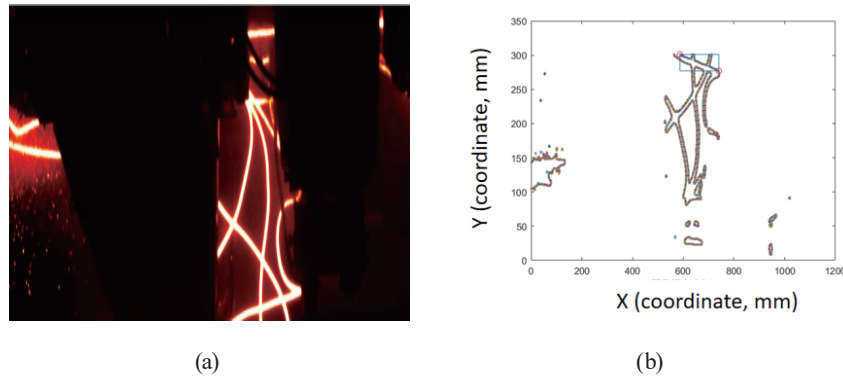

Fig. 12.   (Color online) Pictures of fork-type HSBS accident: (a) picture taken by vision sensors and (b) picture processed by MDPHT.

Then, we obtained the final regional boundary maps via MDPHT as shown in Figs. 11(b) and 12(b), respectively.

Second, we performed two recognition tests (Cases 1 and 2). In Case 1, 50 accident-type images with different HSBS accidents were adopted. In Case 2, 50 normal images with different rotational angles and vibration levels of the sensor lens were adopted. The threshold was set as 0.8 (higher than 0.8 means a normal picture and lower than 0.8 means an abnormal picture) in calculations. Through calculations via MDPHT, we obtained the recognition results for Cases 1 and 2, as shown in Figs. 13 and 14, respectively. In the accident-type image verification case, we found from Fig. 13 that there are four points with PR values greater than 0.8, that is, four images failed to be identified. In the normal image verification case, we found from Fig. 14 that there are nine points with PR values smaller than 0.8, that is, nine images failed to be identified. The identification accuracies of the above two cases are summarized in Table 1. The overall identification accuracy was obtained to be 0.87 using MDPHT.

To sum up, the recognition accuracy of MDPHT is not as expected in general, and this method is especially weak in recognizing pictures taken from a camera with lens vibration or offset. Therefore, we need other comprehensive methods to remedy this shortcoming.
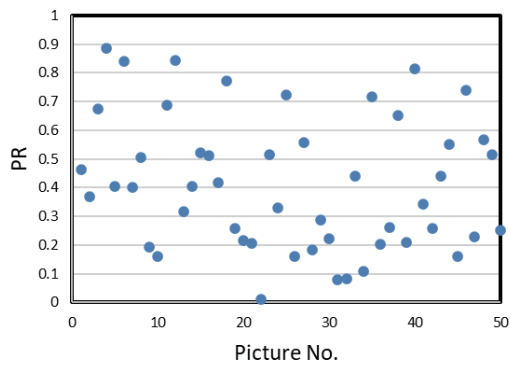
Fig. 13. (Color online) Verification test result of 50 accident-type images with different HSBS accidents by MDPHT.
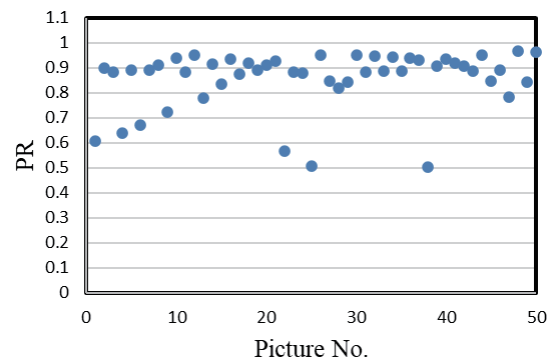

Fig. 14. (Color online) Verification test result of 50 normal images with different HSBS accidents by MDPHT.

Table 1
Identification accuracies of tests by MDPHT.

Image type	Number of pictures	Unsuccessful recognition	Successful recognition	Recognition success rate
Accident-type images (Case 1)	50	4	46	0.92
Normal images (Case 2)	50	9	41	0.82
Sum	100	13	37	0.87 (ave.)

4.2 PHCD

Among the image features, the three most difficult parts are the image edge, the corner point, and the spot. Morphologically, corner points are usually located at the intersection of image edges. From the image pixel perspective, the corner point is a point whose gray value changes considerably in some directions, which is an important basis for PHCD. Because the red-hot steel bar under normal conditions mainly has a four-sided or parallel four-sided contour, we replaced the two corner points with a maximum distance to replace the two points with a maximum distance in calculations. On the basis of the picture of the HSBS accident in Fig. 15(a), we obtained the final regional boundary map via PHCD as shown in Fig. 15(b).

Then, we performed two recognition tests (Cases 3 and 4). In Case 3, 50 accident-type images with different HSBS accidents were adopted. In Case 4, 50 normal images with different rotational angles and vibration levels of the sensor lens were adopted. The PR was chosen as the recognition parameter as usual whose threshold value was set as 0.8 (higher than 0.8 means a normal picture, lower than 0.8 means an abnormal picture) in calculations. Through calculations via PHCD, we obtained the recognition results for Cases 3 and 4, as shown in Figs. 16 and 17, respectively. In the accident-type image verification case, we found from Fig. 16 that there are six points with PR values greater than 0.8, that is, six images failed to be identified. In the normal image verification case, we found from Fig. 17 that there is one point with a PR value smaller than 0.8, that is, one image failed to be identified. The identification accuracies of the above two cases are summarized in Table 2. The overall identification accuracy was obtained to be 0.93 using PHCD.
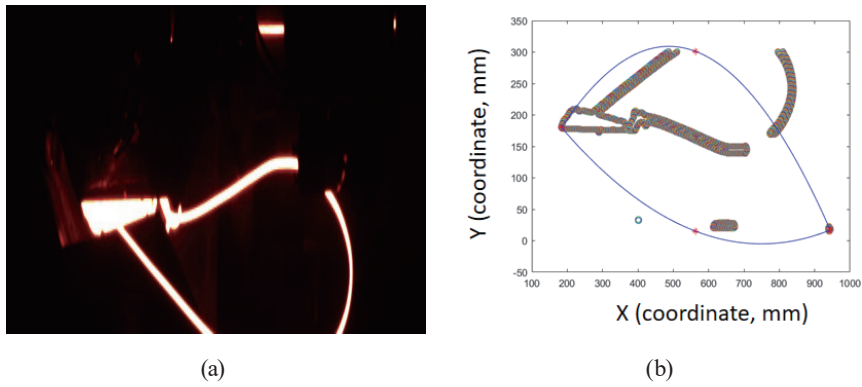
(a) (b)

Fig. 15. (Color online) Pictures of HSBS accidents: (a) picture taken by visual sensors and (b) picture processed by PHCD.
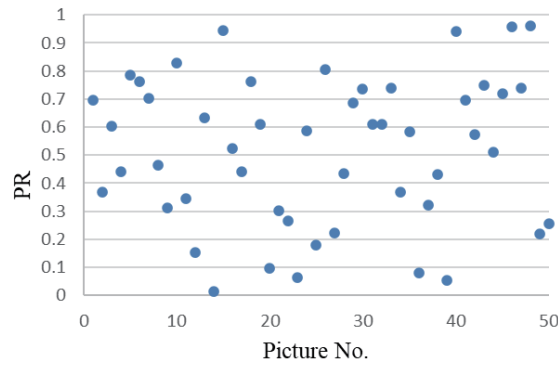

Fig. 16. (Color online) Verification test result of 50 accident-type images with different HSBS accidents by PHCD.
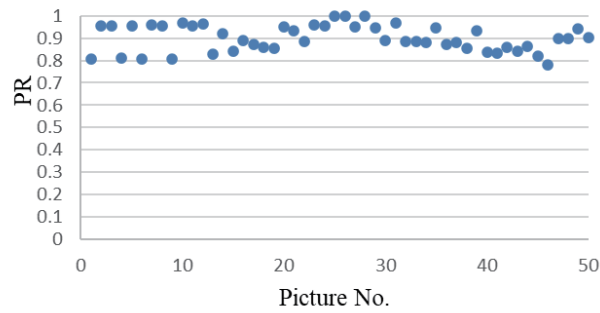

Fig. 17. (Color online) Verification test result of 50 normal images with different HSBS accidents by PHCD.

Table 2
Identification accuracies of tests by PHCD.

Image type	Number of pictures	Unsuccessful recognition	Successful recognition	Recognition success rate
Accident-type images (Case 3)	50	6	44	0.88
Normal images (Case 4)	50	1	49	0.98
Sum	100	7	93	0.93 (ave.)

4.3   CRA

Previous studies have shown that (1) MDPHT is not sufficiently accurate and has strong randomness, especially worse in accident-type image recognition, and (2) PHCD has a poor ability to recognize accident-type images. Therefore, we proposed CRA to overcome the above problems.

On the basis of the picture of an HSBS accident in Fig. 18(a), through calculations via CRA, we obtained a clear regional boundary map, as shown in Fig. 18(b), where the boundary shape of the HSBS can be definitely determined.

Then, we performed two recognition tests (Cases 5 and 6). In Case 5, 50 accident-type images with different HSBS accidents were adopted. In Case 6, 50 normal images with different rotational angles and vibration levels of the sensor lens were adopted. The curvature of the curve in the image (k) is selected as the recognition parameter and its threshold is set to 1.5 (higher than 1.5 means a normal picture and lower than 1.5 means an abnormal picture) in calculations. Through calculations via PHCD, we obtained the recognition results for Cases 5 and 6, as shown in Figs. 19 and Fig. 20, respectively. In the accident-type image verification case, we found from Fig. 19 that there are two points with k values greater than 1.5, that is, two images failed to be identified. In the normal image verification case, we found from Fig. 20 that there are two points

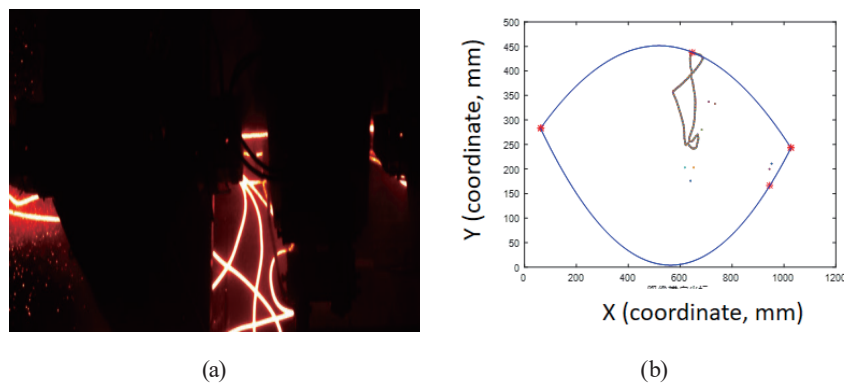| (a) | (b) |

Fig. 18.   (Color online) Pictures of HSBS accidents: (a) picture taken by visual sensors and (b) picture processed by CRA.
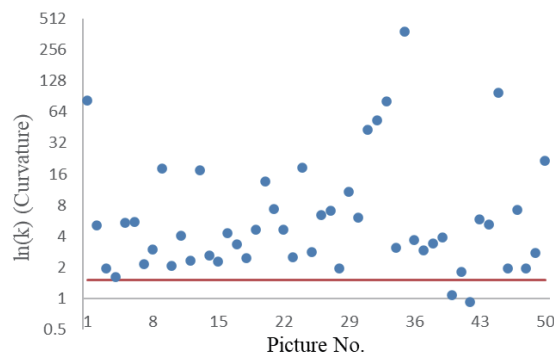

Fig. 19.   (Color online) Verification test result of 50 accident-type images with different HSBS accidents by CRA.
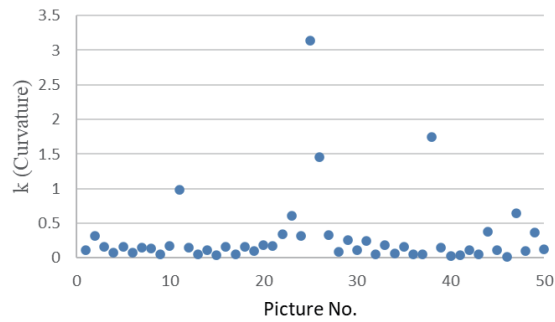
Fig. 20. (Color online) Verification test result of 50 normal images with different HSBS accidents by CRA.

with PR values smaller than 0.8, that is, two images failed to be identified. The identification accuracies of the above two tests are summarized in Table 3. The average identification accuracy obtained was 0.96 using CRA.

4.4 TIOIR method

To overcome the defects of MDPHT, PHCD, and CRA and retain their merits for recognizing HSBS accidents, we integrated these three methods into a three-in-one learning classification method as discussed in the following.

The Bagging method[33–35] is a sampling method with retraction, and its algorithm process is as follows:

Step 1: Extract the training set from the original sample set. Each time, k data is extracted as a training set to obtain a classifier, and *n* classifiers are made. This results in *n* weak classifiers.

Step 2: Use these *n* weak classifiers in parallel, vote with the same weight, and finally obtain the classification result according to the minority obedience to majority.

The core algorithm of the Bagging method is the decision tree scheme. The structure of the decision tree generally starts from the root node, passes through the middle node (non-leaf and root nodes), and moves step by step to the leaf node. All the data will continously branch through the node and finally fall to the leaf node to form the target classification. We used two feature selection methods for the tree root nodes and each intermediate node: Iterative Dichotomiser 3 (ID3) and C4.5 methods, described as follows.

ID3, an algorithm invented by Quinlan,[36] is used to generate a decision tree from the obtained dataset. In ID3, we use the entropy to measure the message gain. The entropy is defined as the uncertainty of a random variable:

$$H = -\sum p \times \log_2 p, \tag{1}$$

where H is the entropy and p is the probability of an event occurring in a set. The greater the entropy, the greater the event uncertainty. Conventionally, ID3 has some defects such as, in some

Table 3
Identification accuracies of tests by CRA.

Image type	Number of pictures	Unsuccessful recognition	Successful recognition	Recognition success rate
Accident-type images (Case 5)	50	2	48	0.96
Normal images (Case 6)	50	2	48	0.96
Sum	100	4	96	0.96 (ave.)

situations, the entropy value becomes too small to be used in calculations. Therefore, we used the C4.5 method under certain conditions.

For C4.5, "C" means that this algorithm is written in C and 4.5 specifies the version of the algorithm. C4.5 is an algorithm used to generate a decision tree developed by Taspinar *et al.*,[37] and it is an extension of Quinlan's earlier ID3 algorithm. In this method, we define the information gain rate as

$$GR(D,a) = \frac{IG(D,a)}{IV(a)}, \tag{2}$$

where *GR* is the information gain rate, *D* is an event, *a* is a feature in event *D*, *IG* is the information gain of feature *a*, and *IV*(*a*) represents the entropy of *a*.

In the Stacking method,[38] first, we made *n* weak classifiers by the Bagging method, and then the outputs of these *n* trained weak classifiers were used as the model inputs with certain weights. The weights are naturally generated by the classifier. Eventually, we can obtain the final model output through calculations. The Boosting method[38] is different from the Bagging method in that it connects multiple weak classifiers in series and integrates the weighted idea of the Stacking method.

In this study, we combined the ideas of equal voting in the Bagging method and tandem classification in the Boosting method with the integration of MDPHT, PHCD, and CRA to form a novel TIOIR method. The manipulation procedure of the TIOIR method is as follows. First, we integrate the MDPHT and PHCD methods to deal with the pictures of HSBS accidents taken at the HSBS rolling site. Second, we vote out the pictures that are different from the majority. Third, we vote through the CRA method to decide on whether the processed picture is normal or is of the accident type. Finally, we obtain the recognition results.

Through the manipulation of TIOIR, we performed the recognition tests of 100 HSBS pictures (Cases 7 and 8). In Case 7, 50 accident-type images with different HSBS accidents were adopted. In Case 8, 50 normal images with different rotational angles and vibration levels of the sensor lens were adopted. The obtained identification accuracies are shown in Table 4. The recognition success rate of the TIOIR method was as high as 97% for accident-type images and 98% for normal images. The overall average recognition success rate was 97%, which means that the TIOIR method is much more accurate than the MDPHT, PHCD, and CRA methods. Hence, the recognition robustness and fault tolerance are considerably improved by using the proposed TIOIR method in HSBS accident detection at a steel-bar rolling site.

Table 4
Identification accuracies of tests by TIOIR method.

Image type	Number of pictures	Unsuccessful recognition	Successful recognition	Recognition success rate
Accident-type images (Case 7)	50	1	49	0.99
Normal images (Case 8)	50	2	48	0.98
Sum	100	3	97	0.97 (ave.)

5. Conclusion

In this study, we proposed a novel TIOIR method to rapidly and accurately recognize the images of HSBS accidents at a steel-bar rolling site. The proposed TIOIR method integrates the merits of MDPHT, PHCD, and CRA. Moreover, for practical applications, we designed and built an image detection and identification system of HSBS accidents, which includes the following six parts: the detecting unit (visual and infrared thermal image sensors), the data processing unit, the data transmitting unit (Ethernet and data exchanger), the data manipulation unit (cloud servers and cloud computers), an alarm unit, and a remote central control unit. The former three units constitute a detection subsystem, and we have four subsystems in total to obtain the images of various HSBS accidents in real time, which are set at the rough, middle, pre-fine, and fine rolling sites. Through the operation of the designed diagnostic system, we found that the average recognition accuracies of MDPHT, PHCD, and CRA are 87, 93, and 96%, respectively. However, the overall and average success rate of the TIOIR method was as high as 97%. Through the operation of the proposed image detection and identification system with an imbedded TIOIR calculation method, we can rapidly and accurately monitor the HSBS accident in the rolling field in real time with a fairly high recognition rate.

Acknowledgments

References

1　D. Bhattacharya, A. Mishra, P. P. Ganga, and S. Misra: Jamshedpur. Case Stud. Eng. Fail. Anal. **5** (2016) 15.
2　Z. Chen, Y.Liu, A. Valera-Medina, and F. Robinson: Proc. Cirp. **81** (2019) 453.
3　X. Liu and H. Xia: J. Mater. Process. Technol. **278** (2020) 116537.
4　A. V. Kozhevnikov, D. L. Shalaevsky, and A. S. Smirnov: J. Chem. Technol. Metall. **55** (2020) 889.
5　S. Zhou, Y. Zeng, S. Li, H. Zhu, X. Liu, and X. Zhang: Appl. Sci. **12** (2022) 8905. https://doi.org/10.3390/app12178905
6　J. Rusnák, P. Malega, J. Svetlík, V. Rudy, and N. Šmajda: Mater. **13** (2020) 3509. https://doi.org/10.3390/ma13163509
7　B. Dominik, C. Yves, L. Maxime, L. Nicolas, P. Luc, B. Romain, and P. J. Philippe: J. Mater. Process. Technol. **296** (2021) 117175. https://doi.org/10.1016/j.jmatprotec.2021.117175
8　J. T. Pater, B. Tomasz, W. Łukasz, M. S. Mikhail: Int. J. Mach. Tools Manuf. **163** (2021) 103706. https://doi.org/10.1016/j.ijmachtools.2021.103706
9　A. Bouguettaya, Z. Mentouri, and H. Zarzour: Int. J. Adv. Manuf. Technol. **125** (2023) 5313. https://doi.org/10.1007/s00170-023-10947-8
10　M. Qian, Z. Wang, J. Zhao, Z. Xiang, P. Wei, and J. Zhang: Measurement **213** (2023) 31. https://doi.org/10.1016/j.measurement.2023.112724
11　I. Ullah and Q. H. Mahmoud: IEEE Access **10** (2022) 62722. http://doi.org/10.1109/ACCESS.2022.3176317
12　V. Sivalingam, R. Elarabi, J. Bhargavi, M. S. Sheela, R. Padmapriya, and A. N. Arularasan: J. Adv. Res. Appl. Sci. Eng. Technol. **31** (2023) 327. https://doi.org/10.37934/araset.31.2.327338
13　H. Liu, S. Wang, G. Jing, Z. Yu, J. Yang, Y. Zhang, and Y. Guo: Sensors **23** (2023) 5383. https://doi.org/10.3390/s23125383
14　J. Yu, A. D. Antonio, and E. V. Mora: Comput. **11** (2022) 26. https://doi.org/10.3390/computers11020026
15　M. Forgione, A. Muni, D. Piga, and M. Gallieri: Automatica **155** (2023) 111092. https://doi.org/10.1016/j.automatica.2023.111092
16　S. Alkadi, S. A. Ahmadi, and M. Ismail: Appl. Sci. **13** (2023) 6001. https://doi.org/10.3390/app13106001
17　K. Teixeira, G. Miguel, H. S. Silva, and F. Madeiro: IEEE Access **11** (2023) 117582. http://doi.org/10.1109/ACCESS.2023.3326101
18　Z. Xu and J. H. Saleh: Reliab. Eng. Syst. Saf. **211** (2021) 107530. https://doi.org/10.1016/j.ress.2021.107530
19　D. P. Abhishek and R. Jegadeeshwaran: Measurement **173** (2021) 108649. https://doi.org/10.1016/j.measurement.2020.108649
20　F. Yanzhou, R. J. D. Austin, Y. Lang, Z. Tianyu, P. Avery, and B. Yunusa: J. Manuf. Processes **75** (2022) 693. https://doi.org/10.1016/j.jmapro.2021.12.061
21　M. F. Khan, A. Alam, M. A. Siddiqui, M. S. Alam, Y. Rafat, N. Salik, and I. A. Saidan: Mater. Today: Proc. **42** (2021) 521. https://doi.org/10.1016/j.matpr.2020.10.482
22　D. Goyal, S. S. Dhami, and B. S. Pabla: IEEE Sens. J. **20** (2020) 4816. http://doi.org/10.1109/JSEN.2020.2964633
23　T. Benbarrad, M. Salhaoui, S. B. Kenitar, and M. Arioua: J. Sens. Actuator Netw. **10** (2021) 7. https://doi.org/10.3390/jsan10010007
24　A. H. Safaie, H. Rastiveis, A. Shams, W. A. Sarasua, and J. Li: ISPRS J. Photogramm. Remote Sens.**174** (2021) 19. https://doi.org/10.1016/j.isprsjprs.2021.01.026
25　R. Li, D. Shi, Y. Zhang, K. Li, and R. Li: 2019 IEEE/RSJ Int. Conf. Intell. Rob. Syst. (IROS, 2019) 6223. http://doi.org/10.1109/IROS40897.2019.8968491
26　M. Wan, X. Ye, X. Zhang, Y. Xu, G. Gu, and Q. Chen: IEEE Geosci. Remote Sens. Lett. **19** (2022) 1. http://doi.org/10.1109/LGRS.2021.3051183
27　G. Tuysuzoglu and D. Birant: Int. Arab J. Inf. Technol. **17** (2020) 515. http://doi.org/10.34028/iajit/17/4/10
28　L. Benedetti, M. Corsini, P. Cignoni, M. Cignoni, M. Callieri, and R. Scopigno: Mach. Vision Appl. **23** (2012) 327. https://doi.org/10.1007/s00138-010-0304-x
29　W. Q. Wang: Adv. Eng. Forum **1** (2011) 283. http://doi.org/10.4028/www.scientific.net/aef.1.283
30　P. Kannan, S. Deepa, and R. Ramakrishnan: Am. J. Intell. Syst. **2** (2012) 141. http://doi.org/10.5923/j.ajis.20120206.01
31　W. Chen, T. Zuo, and Z. Ye: 2023 IEEE Int. Conf. Image Process. Comput. Appl. (ICIPCA, 2023) 832. https://doi.org/10.1109/ICIPCA59209.2023.10257928
32　A. Safaie, H. Rastiveis, A. Shams, W. A. Sarasua, and J. Li: ISPRS J. Photogramm. Remote Sens. **174** (2021) 19.

33	G. Rani, S. Srivastava, N. Kundu and V. S. Dhaka: 2023 Int. Conf. Emerging Trends Networks Comput. Commun. (ETNCC, 2023) 229. https://doi.org/10.1109/ETNCC59188.2023.10284977

34	Q. An, X. Chen, H. Wang, H. Yang, Y. Yang, W. Huang, and L. Wang: Fractal Fract. **6** (2022) 95. https://doi.org/10.3390/fractalfract6020095

35	M. Fahad, H. Sharif, F. Rehman, Z. Bilal, S. Ahmad, and H. Maqsood: 2022 3rd Int. Conf. Innovations Comput. Sci. Software Eng. (ICONICS, 2022) 1. https://doi.org/10.1109/ICONICS56716.2022.10100486

36	J. R. Quinlan: Mach. Learn. **1** (1986) 81. https://doi.org/10.1023/A:1022643204877

37	Y. S. Taspinar, C. Ilkay, and K. Murat: J. X-Ray Sci. Technol. **30** (2022) 73.

38	R. A. Mohammad, A. S. Sayed, N. Hamid, and E. Samaneh: Comput. Electr. Eng. **103** (2022) 108382. https://doi.org/10.1016/j.compeleceng.2022.108382